Single Fiber OCT-based Retina Detection for Robot-assisted Retinal Vein Cannulation

G. Borghesan*, D. Bouget*, E. Lankenau†, R. Neffin†, P. Koch‡,
K. Willekens§, P. Stalmans§, D. Reynaerts*, E. Vander Poorten*
*Dept. of Mechanical Engineering, KU Leuven, †OptoMedical Technologies GmbH, Lübeck, Germany
‡Medical Laser Center Lübeck, Lübeck, Germany, §Dept. of Ophthalmology, University of Leuven
gianni.borghesan@kuleuven.be

***Abstract*—Vitreo-retinal surgery concerns a set of particularly demanding micro-surgical interventions that take place at the back of the eye. Expert micro-surgeons are to manipulate fragile membranes or vessels while taking great care not to damage the underlying retina. Despite using high quality stereo microscopes, depth perception remains limited. Efforts have been conducted to enhance depth awareness through adding OCT or even force sensing. Whereas OCT has been predominantly used to assist in retinal membrane peeling procedures, so far little work has been conducted to use it for offering assistance during retinal vein cannulation. This abstract describes some first results of a novel algorithm that has been designed to reliably estimate the distance to the retina from an instrument with integrated OCT-fiber. However, it is anticipated that the algorithm can be further expanded to estimate other useful characteristics as well. It could for example help to automatically detect vessels on the retina, or to estimate the diameter or center of a targeted vessel. Equipped with this knowledge more sophisticated assistive control schemes could be designed to further increase cannulation reliability.**

I. Introduction

Vitreo-retinal (VR) surgery is currently performed in a fully manual manner. Upon start of the procedure the surgeon carefully puts up to four trocars into place at 3 to 4 mm from the corneal limbus, the border between the cornea and the sclera (Fig.1). Through these trocars thin instruments are inserted to operate on the interior part of the eye. The micro-surgeon observes the retina and relative instrument motion via a stereo-microscope positioned above the patient's eye. From the binoculars the optical path goes through the different lenses of the stereo-microscope, additional wide-angle lenses such as the EIBOS (Haag-Streit Surgical GmbH, Rosengarten, Germany), the BIOM®(Oculus Surgical, Florida, US) or contact lenses, the natural lens of the patient and finally through the vitreous humour a gel-like substance that occupies the interior volume of the eye-ball[1]. The complex optical path and the difficulty of getting sufficient light through small incisions at the target site, severely limit the surgeon's depth perception. Given the small size of the structures the micro-surgeon is to deal with - for *epiretinal membrane peeling* (ERM-peeling) a membrane up to about 60μm is to be peeled off; for ILM peeling the *internal limiting membrane* is only about 4μm thick; veins that are to be cannulated to treat *retinal vein occlusion* typically have diameters in the order of 100μm - it is clear that inaccurate depth perception and depth control can cause serious complications [1], [2]. Accordingly significant research has been conducted to improve depth perception through adoption of alternative sensing techniques. OCT and force sensing are some of the more mature techniques that have been investigated.

[1]If that was not replaced by mineral oil.

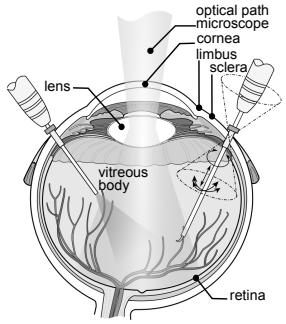

Fig. 1. Anatomy of the eye, focus on structures relevant for VR surgery.

II. Goals and Related work

OCT images have been previously employed in a number of algorithms targeting, for example, automatic segmentation of retinal layers [3]; detection of vessels [4] or to identify markers that predict certain diseases [5]. Most of these results rely on 2D or 3D OCT images, referred to as B- and C-scans respectively. This data is obtained from a scanner that is mounted at the far end of the complex optical path. Similar to [7] we aim to employ OCT data that is acquired via an optical fibre incorporated directly inside the surgical instrument. By doing so the complex optical path can be by-passed and direct i.e. more accurate measurements of the retina can be obtained. Only a single ray of laser light can be passed at a time through the laser fiber offering a one-dimensional depth aka A-scan. In order to reconstruct a larger surface the instrument could be controlled to make a scanning pattern. Despite the improved accuracy, the obtained signal remains quite noisy and the limited field of view, i.e. absence of a broader context, necessitates adequate filtering to use this kind of data in critical applications such as robotic control loops.

Balicki *et al.* implemented such approach when mounting an OCT probe on an micro-surgical pick [7]. The experiments reported by Balicki *et al.* however are conducted on synthetic phantoms and therefore the signals that are employed are much less noisy than the signals one typically gets. The objective of this work consists in evaluating the feasibility of using A-scans for robustly identifying the upper layer of the retina in a more realistic setting. Here, noisy OCT data from ex-vivo pig

eyes is employed and a novel algorithm to deal with this data is proposed. Note, although the proposed approach is used to detect membrane layers, the proposed approach is more general and is believed to be also helpful in discriminating the location of vessels on top of or even below the retinal surface. With only very limited loss of generality B-scans (fig. 2) are employed to test the concept. Each time only a single line of these B-scans is used, simulating a corresponding A-scan. By removing the vitreous humour and the lenses from an ex-vivo pig eye and EIBOS, the obtained lines from these B-scans approximate A-scans closely. To filter out the noisy artefacts a methodology similar to the one employed in [8] is adopted. The method employs *probabilistic principal component analysis* (ppca, [9]) to characterize a number of *latent* variables. In the following sections the algorithm and some experimental results are introduced.

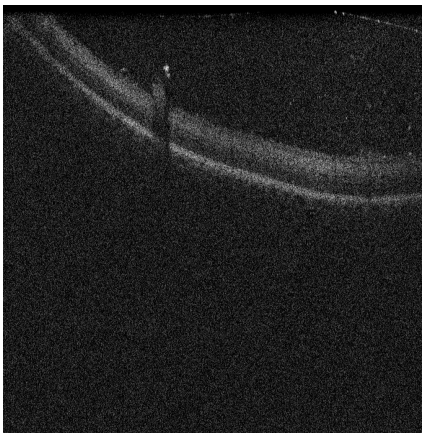

Fig. 2. Example of B-scan; as A-scan, a single vertical line of the image is considered. Each image has 1000 lines, each composed of 1024 depth pixels.

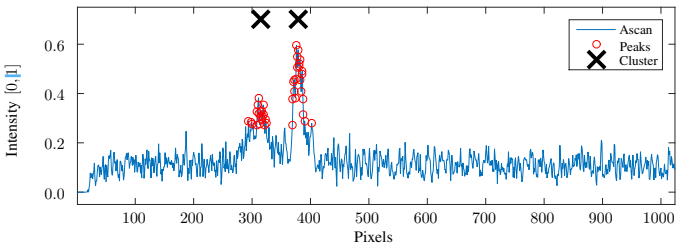

Fig. 3. Peak detection and clustering are the initial step for normalising the data. The data is averaged on 8 images taken consecutively to reduce noise.

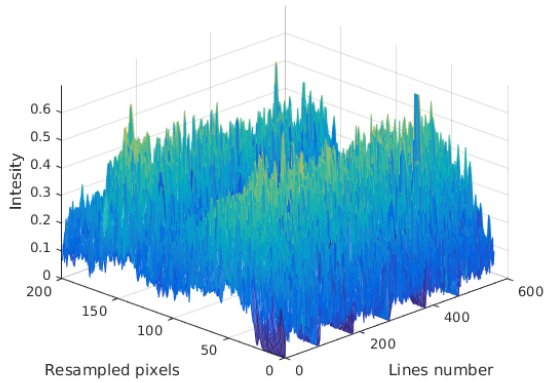

Fig. 4. Data set used in ppca.

III. Proposed algorithm

The proposed procedure consists of a learning phase (off-line, that makes use of more than one line at a time) and a run-time identification phase (using a single line, as produced by an OCT fiber probe). Both phases are described next.

A. Learning phase

Ppca needs a normalised training set (i.e. each pixel must represent the same information). To achieve this, we extract in a semi-automatic way some landmarks around important features. The data set is then re-sampled in such a way that these landmarks appear in the same area.

In the first phase 6 sets of B-scans (from ex-vivo porcine eyes, each set taken on a given position) are averaged to reduce noise. Then peaks (brightest pixels) are used to identify the center of a membrane layer. In the current image (fig. 2) two layers are visible. k-means is used to cluster these pixels into 2 clusters. The results of these operations are shown in fig. 3. The procedure is run on a whole image. Then we consider the distance between the 2 clusters as a representative measure and discard outliers. From the selected line samples, the region around the average distance, with a span equal to twice the distance between the clusters is selected, and re-sampled on a fixed span of 200 pixels. The resulting data set is represented in fig. 4. From the ppca only two latent variables are kept.

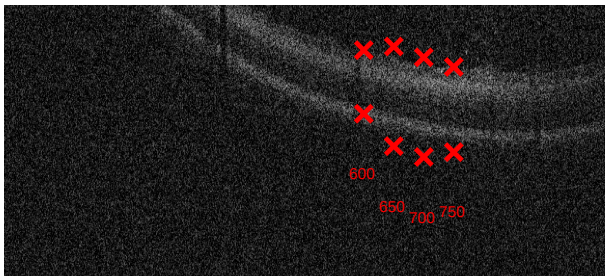

(a) Representation of P_0 and $P_0 + \Delta P$ computed after initialization.

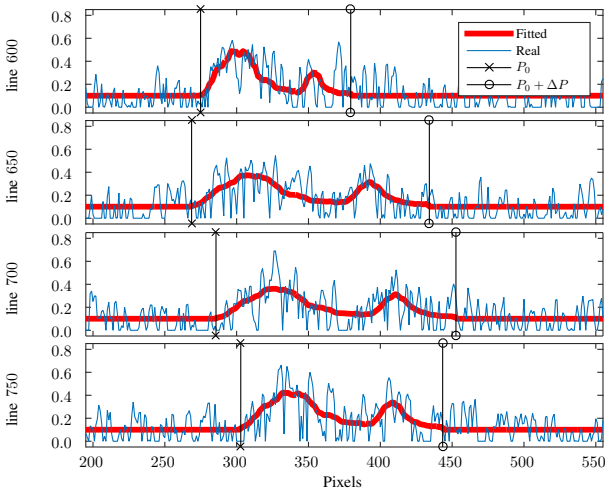

(b) Fitting of the profile

Fig. 5. Results of iterating the UKF on the same input data in the initialization phase. The red fat line represents the expected output.

B. Filter initialization and run-time execution

In order to track the position of the retinal layers in the image an unscented Kalman filter is used. The filter states are the initial pixel that maps in pixel 1 of the dataset (P_0), the number of pixels that maps in the whole data set (ΔP), and the two latent variables (x_l). The expected measurements are computed as follows: first, the modes are multiplied by x_l, then, the points are stretched and translated as dictated by P_0 and ΔP, lastly, the output is re-sampled between 1 and 1024 (the size of the sensor measurement), using a default value for the part of the image that is outside the $[P_0, P_0 + \Delta P]$ interval.

One of the most critical parts is to determine which parameters to use to initialise the filter. In this regard, we employ the same rationale used in the data set segmentation, *e.g.* peak detection and clustering. In order to allow the filter to converge, several update iterations (30–60) are executed with the same measurement. Four examples of initialised filters are depicted in fig. 5.

C. Filter execution on varying measurements

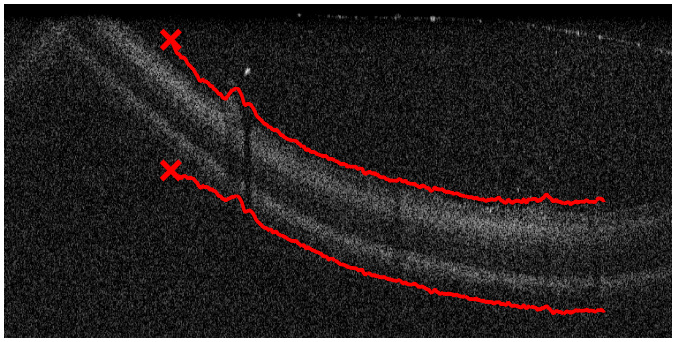

(a) Overlay of P_0 and $P_0 + \Delta P$ on OCT B-scan.

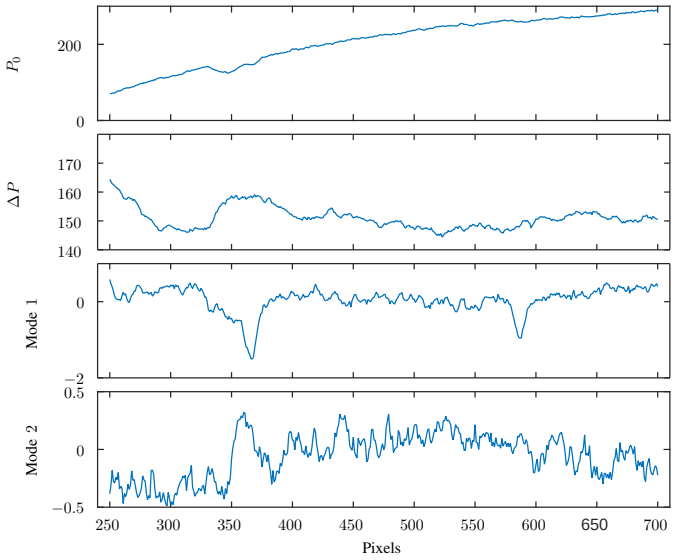

(b) Values of the UKF variables.

Fig. 6. Example of a filter executed with a time varying input. After initialization (results in red crosses), at each time step the filter is moved one pixel to the right. The data reported in red are $[P_0, P_0 + \Delta P]$

In order to test the proposed filter in a situation more similar to reality, but yet enough controlled to be able to evaluate the results, a B-scan was employed, and an single input line was used for each iteration, shifting one pixel each time, simulating a horizontal movement of the OCT fiber probe. For small travel this motion is fairly representative. The overall results for this scan are reported in fig. 6. It can be observed qualitatively that at locations artefacts are present, the values of Mode 1 changes drastically. This suggests that analysis of the state can be used to classify tissue and e.g. detect the presence of vessels or other features.

IV. Conclusion

This abstract presented a way to formalise an UKF to track the position of the retina. The approach takes advantage of the structure present in retinal layers, in contrast to [7], to get a robust estimate of the distance to the surface. While the presented results are still preliminary, the filter showed good robustness to artefacts and noise. Two main drawbacks should be pointed out: first of all, the filter is strongly influenced by the numerous local minima; for this reason, wrong initialization can cause the filter to converge to a wrong state. At this end, at least the initialization could be delegated to a global search method, such as a particle filter. Secondly, the filter was not trained on vessels. In fact a number of filters could be operated in parallel each trained with specific data-sets e.g. one that focuses on vessels, to discriminate those from retinal layers.

Acknowledgment

Research funded by The EU Framework Programme for Research and Innovation - Horizon 2020 - Grant Agreement No 645331.

References

[1] R. Sjaarda, B. Glaser, J. Thompson, R. Murphy, and A. Hanham, "Distribution of iatrogenic retinal breaks in macular hole surgery," *Ophthalmology*, vol. 102, no. 9, pp. 1387–1392, 1995.

[2] K. Nakata, M. Ohji, Y. Ikuno, S. Kusaka, F. Gomi, and Y. Tano, "Sub-retinal hemorrhage during internal limiting membrane peeling for a macular hole," *Graefe's Archive for Clinical and Experimental Ophthalmology*, vol. 241, no. 7, pp. 582–584, 2003. [Online]. Available: http://dx.doi.org/10.1007/s00417-003-0676-y

[3] A. Yazdanpanah, G. Hamarneh, B. R. Smith, and M. V. Sarunic, "Segmentation of intra-retinal layers from optical coherence tomography images using an active contour approach," *IEEE Transactions on Medical Imaging*, vol. 30, no. 2, pp. 484–496, Feb 2011.

[4] S. Lu, C. Y. l. Cheung, J. Liu, J. H. Lim, C. K. s. Leung, and T. Y. Wong, "Automated layer segmentation of optical coherence tomography images," *IEEE Transactions on Biomedical Engineering*, vol. 57, no. 10, pp. 2605–2608, Oct 2010.

[5] R. Kafieh, H. Rabbani, and S. Kermani, "A review of algorithms for segmentation of optical coherence tomography from retina," *J Med Signals Sens*, vol. 3, no. 1, pp. 45–60, 2013.

[6] A. Gijbels, N. Wouters, P. Stalmans, H. Van Brussel, D. Reynaerts, and E. V. Poorten, "Design and realisation of a novel robotic manipulator for retinal surgery," in *Intelligent Robots and Systems (IROS), 2013 IEEE/RSJ International Conference on*. IEEE, 2013, pp. 3598–3603.

[7] M. Balicki, J.-H. Han, I. Iordachita, P. Gehlbach, J. Handa, R. Taylor, and J. Kang, "Single fiber optical coherence tomography microsurgical instruments for computer and robot-assisted retinal surgery," in *Medical Image Computing and Computer-Assisted Intervention–MICCAI 2009*. Springer, 2009, pp. 108–115.

[8] E. Aertbeliën and J. de Schutter, "Learning a predictive model of human gait for the control of a lower-limb exoskeleton," in *5th IEEE RAS/EMBS International Conference on Biomedical Robotics and Biomechatronics*, Aug 2014, pp. 520–525.

[9] M. E. Tipping and C. M. Bishop, "Probabilistic principal component analysis," *Journal of the Royal Statistical Society, Series B*, vol. 61, pp. 611–622, 1999.